



HAL
open science

Physicochemical and electrical characterizations of atomic layer deposition grown HfO(2) on TiN and Pt for metal-insulator-metal application

Corentin Jorel, Christophe Vallée, Emmanuel Gourvest, Bernard Pelissier, Marceline Bonvalot, Maurice Kahn, Patrice Gonon

► To cite this version:

Corentin Jorel, Christophe Vallée, Emmanuel Gourvest, Bernard Pelissier, Marceline Bonvalot, et al.. Physicochemical and electrical characterizations of atomic layer deposition grown HfO(2) on TiN and Pt for metal-insulator-metal application. *Journal of Vacuum Science & Technology B Microelectronics and Nanometer Structures*, 2009, 27 (1), pp.378. 10.1116/1.3021036 . hal-00633071

HAL Id: hal-00633071

<https://hal.science/hal-00633071>

Submitted on 17 Oct 2011

HAL is a multi-disciplinary open access archive for the deposit and dissemination of scientific research documents, whether they are published or not. The documents may come from teaching and research institutions in France or abroad, or from public or private research centers.

L'archive ouverte pluridisciplinaire **HAL**, est destinée au dépôt et à la diffusion de documents scientifiques de niveau recherche, publiés ou non, émanant des établissements d'enseignement et de recherche français ou étrangers, des laboratoires publics ou privés.

Physicochemical and electrical characterizations of atomic layer deposition grown HfO₂ on TiN and Pt for metal-insulator-metal application

C. Jorel,^{a)} C. Vallée,^{b)} E. Gourvest, B. Pelissier, M. Kahn, M. Bonvalot, and P. Gonon
*Laboratoire des Technologies de la Microélectronique (LTM), UMR CNRS 5129, CEA-LETI,
17 rue des Martyrs, 38054 Grenoble Cedex 9, France*

(Received 7 June 2008; accepted 8 September 2008; published 9 February 2009)

This work reports on the study of two HfO₂ metal-insulator-metal structures using two different bottom metal electrodes: Pt and TiN. Different spectroscopic techniques had been used for the physicochemical characterization in order to study the junction interface and determine the oxide thickness and crystallinity: parallel angle resolved x-ray spectroscopy, vacuum ultraviolet ellipsometry, and attenuated total reflectance. Electrical characteristics of the structures with different oxide thicknesses and an evaporated gold counterelectrode are shown. Best results for very thin HfO₂ films in terms of voltage linearity are obtained with the platinum electrodes. This is correlated with differences observed between the continuous conductivity when using Pt electrode instead of TiN electrode. © 2009 American Vacuum Society. [DOI: 10.1116/1.3021036]

I. INTRODUCTION

Meta-insulator-metal (MIM) capacitors are key components of electronic circuits that are used for filtering, decoupling, analog-to-digital conversion, and other radio frequency functions. The actual downscaling of electronic devices implies to substitute the traditional SiO₂ dielectric for new insulating materials with a higher dielectric constant.¹ These materials shall lead to a high capacitance value (≥ 10 fF/ μm^2) with a good voltage linearity (≤ 100 ppm/V²) and low leakage current ($\leq 10^{-7}$ A/cm²).² In MIM devices, the capacitance voltage relationship can be expressed as a second order polynomial equation:

$$\frac{\Delta C}{C_{\min}} \times 10^6 = \left[\frac{C(V) - C_{\min}}{C_{\min}} \right]_{\text{ppm}} = \alpha V^2 + \beta V,$$

where C_{\min} is the minimal capacitance (near zero bias), α and β are, respectively, the quadratic and linear coefficients. Several high- κ dielectric materials or high κ stacks have been investigated such as Ta₂O₅,³ Y₂O₃,⁴ HfO₂,⁵ TiHfO₂,⁶ PrTi_xO_y,⁷ Al₂O₃-HfTiO, ⁸ HfNO-SiO₂-HfTiO,⁹ SrTaO,¹⁰ or TiSiO₄¹¹ but the very thin oxide thickness necessary to obtain large capacitance density implies a degradation of the voltage linearity.

According to some reports^{8,12-14} it is shown that the quadratic coefficient varies with electrodes for a same insulated material. Recently, Yip *et al.*¹⁵ showed how the metal contacts can influence the electrical characteristics of Al₂O₃ MIM capacitors. The physical origin of this voltage nonlinearity can be explained by electrode polarization mechanism.^{13,16} In such a model, mobile carriers form an accumulation layer at the electrode interface, leading to a double layer capacitance which depends on voltage. These mobile carriers were invoked to be oxygen vacancies that are inherently created during oxide growth. Robertson *et al.*¹⁷

recently showed that using high work function electrode metals may help to promote poor oxygen vacancy. Moreover, the apparition of interfacial oxidized form of the metal electrode at the oxide interface has a big impact on the electrical behavior. For example, Wenger *et al.*¹⁸ studied the TiO_z-TiO_xN_y interfacial layer which appears on TiN: considering a relative permittivity of 6, he obtained a quadratic coefficient of 3800 ppm/V² and a 1 nm thickness for this interfacial layer. Assuming a double layer without electrical charges at the interface, the global value of α for the stack varies finally with the equivalent oxide thickness (EOT) and α value of each layer,¹⁹

$$\alpha = \alpha_1 \left(\frac{\text{EOT}_1}{\text{EOT}_{\text{stack}}} \right)^3 + \alpha_2 \left(\frac{\text{EOT}_2}{\text{EOT}_{\text{stack}}} \right)^3.$$

A double layer MIM capacitor may be used to improve the overall linearity,^{19,20} while in case of high k deposition on TiN, the TiO_x-TiO_xN_y layer tends to degrade the linearity.¹⁸

In this article we compare two-metal-HfO₂ stack: TiN-HfO₂ and Pt-HfO₂, HfO₂ being grown in the same condition by atomic layer chemical vapor deposition (AL-CVD). Both physicochemical and electrical characterizations of the structure will be analyzed.

II. SAMPLE PREPARATION

Highly doped 200 mm silicon substrates with controlled (<1 nm) surface thermal oxide were used as wafer for both structures. On the one hand, the 100 nm Pt layer is sputtered at room temperature on a Ti 10 nm seeding layer. On the other hand, the 60 nm TiN layer is deposited by PVD at 350 °C on a 40 nm Ti seeding layer. The Ti layer itself is deposited on a (buffered oxide etch) precleaned wafer. A 20 s postannealing at 720 °C is also performed. Then the HfO₂ layers are deposited at 350 °C and 1 torr by AL-CVD with alternate cycles of H₂O and HfCl₄ precursors. The top gold

^{a)} Author to whom correspondence should be addressed; electronic mail: corentin.jorel@cea.fr

^{b)} Electronic mail: christophe.vallee@cea.fr

electrodes used for electrical measurements were deposited by electron beam evaporation through a shadow mask at 0.5 nm/s.

III. INSULATOR PHYSICOCHEMICAL CHARACTERIZATION

Three main spectroscopic techniques were used for the metal-insulator stack study. The parallel angle resolved x-ray spectroscopy (PARXPS) is a new powerful spectroscopic method for characterizing the chemical bonding states of elements and their evolution in the first 3–7 nm. While allowing the simultaneous acquisition of a great number of angle's intervals, it gives access to depth resolved information in a nondestructive way. Attenuated total reflectance (ATR) has been shown to be a good tool for studying the HfO_2 crystallinity,^{21,22} while vacuum ultraviolet (vuv) ellipsometry allows determining precisely the oxide thickness and an effective “optical” gap. It also confirms the HfO_2 crystallinity.

A. XPS studies of the insulator and back-electrode insulator boundaries

PARXPSs were performed, using a customized Thermo Fisher Scientific Theta 300 spectrometer, with small thickness (<2 nm) HfO_2 layer in order to be able to look at the metal-insulator interface without any etching. In fact, first studies were led with real devices and thicker films: they used the XPS focalized Ar ion beam to dig the oxide layer down to the interface and follow the chemical evolution. However evidence was found that despite the smoothest etching procedure, the Hf chemical environment evolution was not intrinsic (it shows oxygen progressive depletion along the depth), but actually linked to the milling, through Hf–O bonds breaking.

We obtained the typical Hf 4f spectra of HfO_2 on both Pt and TiN at the different angle intervals. No chemical evolution with the electron take-off angle has been observed confirming the chemical stability and homogeneity of the HfO_2 down to the interface. Rigid constraints were used to set the relative shape of the doublet peaks and the energy separation of the two-spin-orbit contribution. A close look at the shape and fitting parameter of the two Hf 4f spectra shows slightly wider peaks in the TiN case and a possible missing contribution at lower energy. This should be considered as an indicator of a very small dispersion of the Hf oxidation state toward oxygen depleted HfO_2 (on the TiN).

In the Pt case, we obtained a perfect handbook shape which rules out the existence of a defined oxidized interfacial layer between Pt and HfO_2 . In the TiN case, the contribution of both oxidized TiO_z and TiO_xN_y could be identified. The energy resolution and the probable oxidation dispersion prevent us to establish the stoichiometry of those states even if the TiO_x one is clearly near the TiO_2 referenced binding energy band.²³ As before, rigid constraints were used to set the relative shape of doublet peaks and their energy separation. A relative depth plot using the direct ratio between the peak intensity at low (20° – 30° , surface and bulk contribution) and high angle (60° – 70° , surface contribution) referred

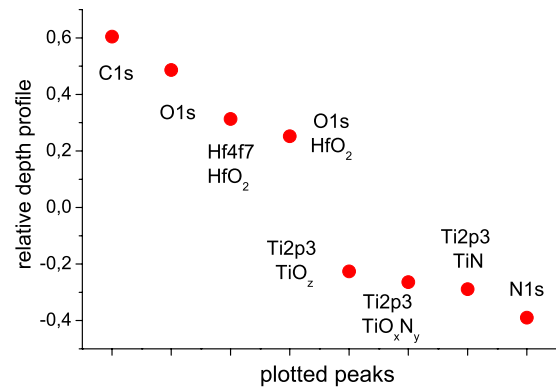


FIG. 1. (Color online) Relative depth plot of the different components. Each peak is related, if possible, to a component chemical bonding. The direct ratio of peak intensity in two collection angle intervals (low angles, full analyzed layer contribution/high angle, surface contribution) is used. First two points are expected C and O surface pollution. Then there is the defined layer of HfO_2 (Hf and O peaks). The last four points are related to the oxidized TiN interfacial layer and to the TiN layer.

to the wafer normal is presented Fig. 1. It shows that the Ti(N) oxidized states are effectively located at the interface. The atomic percentages were calculated thanks to the fitting parameter and Scofield factors (which characterize the element photoemission section). TiN, TiO_xN_y , and TiO_x represent (in the full analyzed layer contribution) 55%, 33%, and 12% of the Ti content.

B. HfO_2 attenuated total reflectance

The ATR spectra in the range of 650 – 800 cm^{-1} concerning the Hf–O–Hf chemical bonds are shown Fig. 2. The different film thicknesses are represented: 11, 7 and 5 nm on Pt and 18, 8, 3, and (\sim)1 nm on TiN. The large band detected for the two thinner films on TiN are associated with an amorphous HfO_2 even though this technique does not clearly discriminate the orthorhombic and amorphous phases: for those very thin films deposited at 350°C without postannealing, the orthorhombic phase may not be present. The other two thicker films show the clear increase in the monoclinic signature with thickness: one peak at 675 cm^{-1} and a smaller one at 775 cm^{-1} . In the case of Pt, we see that even the thinner film is already partially crystallized in the monoclinic phase. It is also significant to see that the 7 nm film has a more monoclinic signature than the 11 nm one, indicating the possible growth of an orthorhombic phase.

C. HfO_2 ellipsometry

We characterize hafnium oxide using vuv spectroscopic ellipsometry from Horiba Jobin Yvon phase modulated spectroscopic ellipsometer. Spectra are recorded between 1.5 and 8 eV with an incident angle of 70° . HfO_2 dielectric function ($\epsilon = \epsilon_1 + i\epsilon_2$) is simulated using a modified Tauc–Lorentz law²⁴ with two oscillators^{25–27} for the imaginary part of the dielectric function while the real part is derived from the expression of ϵ_2 using the Kramers–Kronig dispersion relation as expressed in the following:

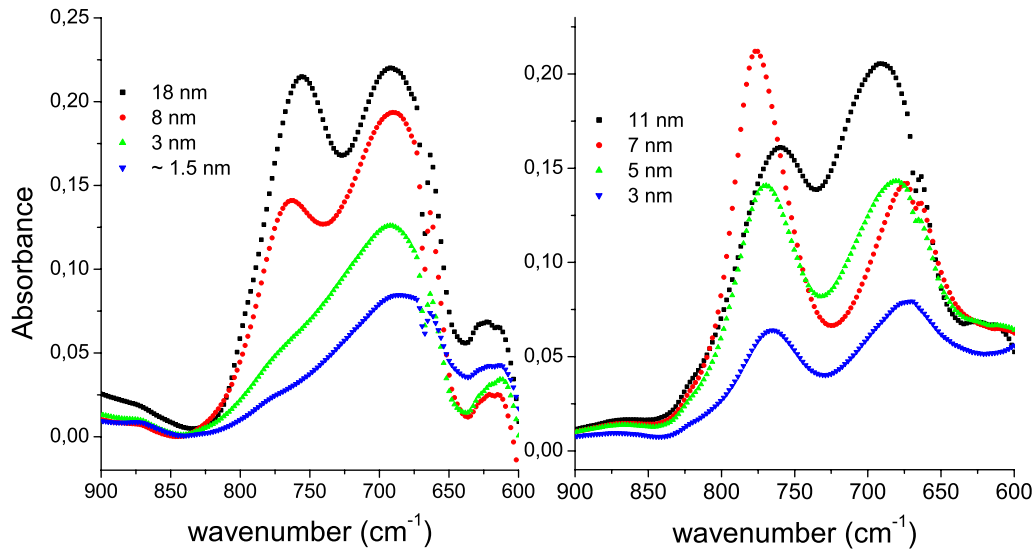


FIG. 2. (Color online) ATR spectra of four HfO₂ films on TiN (left) and Pt (right).

$$\varepsilon_2 = \begin{cases} 0 & (E \leq E_g) \\ \frac{1}{E} \left(\frac{A_1 E_1 C_1 (E - E_g)^2}{(E^2 - E_1^2)^2 + C_1^2 E^2} + \frac{A_2 E_2 C_2 (E - E_g)^2}{(E^2 - E_2^2)^2 + C_2^2 E^2} \right) & (E > E_g) \end{cases},$$

$$\varepsilon_1 = \varepsilon_\infty + \frac{2}{\pi} P \int_0^{+\infty} \frac{\xi \varepsilon_2(\xi)}{\xi^2 - E^2} d\xi,$$

where A_1 and A_2 are related to the strength of the corresponding oscillators (transition matrix elements), C_1 and C_2 are broadening terms, E_1 and E_2 are the peak transition energies, and E_g is the band gap. The imaginary part of the

dielectric function of HfO₂ films deposited on Pt and on TiN obtained from ellipsometric measurements are reported versus the photon energy in Fig. 3. Very small differences are observed between the respective dielectric functions when

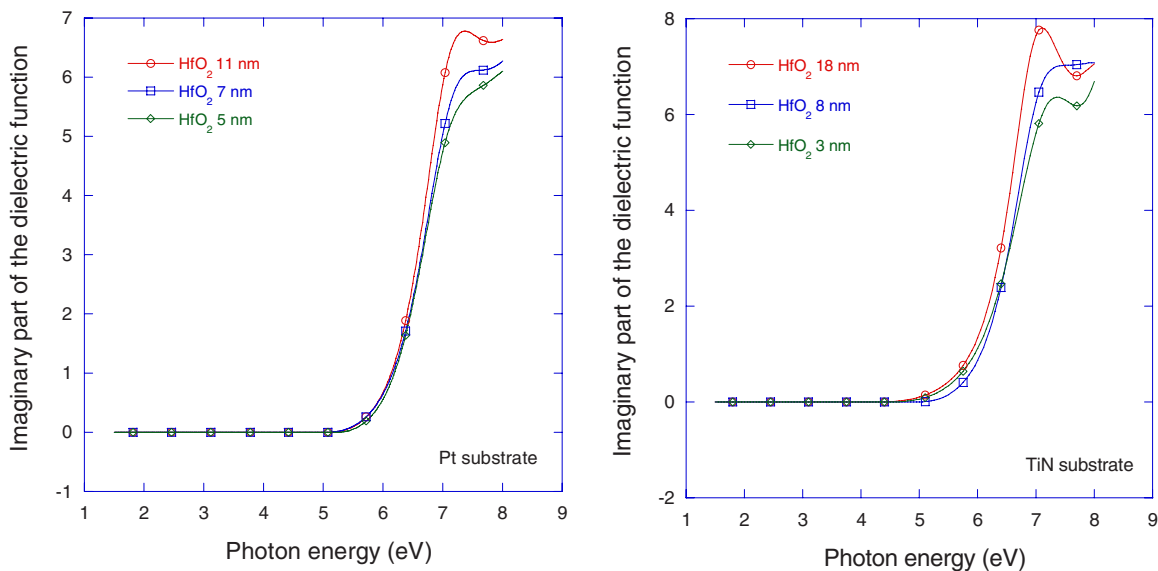


FIG. 3. (Color online) Imaginary part of the dielectric function (ε_2) vs photon energy for the HfO₂ on Pt (left) and TiN (right) films. The optical gap and the film thickness are deduced from the fit.

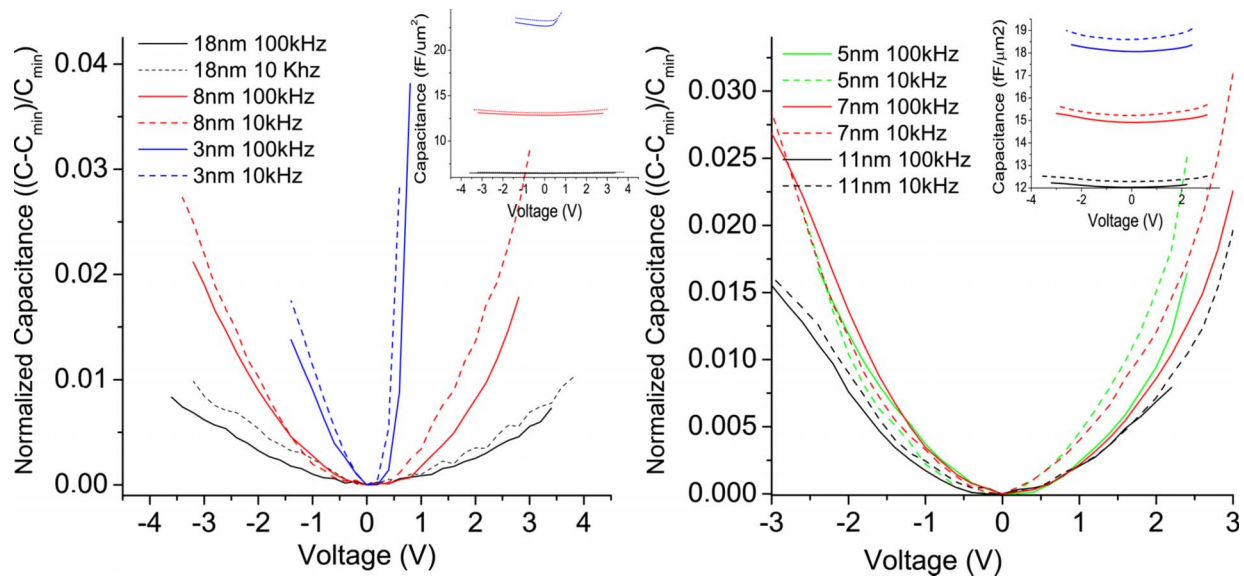


FIG. 4. (Color online) Normalized capacitance $(C-C_{\min})/C_{\min}$ vs voltage for three different thicknesses of HfO_2 on TiN (left) and Pt (right). Corresponding capacitance density vs voltage are shown in the insets.

considering the thickness and/or the substrate material. All shapes are consistent with crystallized material, with structure peaks in good agreement with ATR spectra. Moreover, most of the absorption region fits to a Tauc law characteristic of an indirect band gap²⁸ and the optical band gaps extracted from these fits are all about 5.5 eV. The HfO_2 film thicknesses were calculated on the metal with the interfacial layer contribution, meaning that the 11, 7, and 5 nm HfO_2 on Pt and 18, 8, and 3 nm of HfO_2 on TiN presented in this work, do not include the interfacial layers. We do not observe the presence of a shoulder around 6 eV, which is usually reported for polycrystalline HfO_2 films^{22,29} and identified, as the E_g , T_{2g} states in the band diagram of crystal field splitting hypothesis.³⁰

IV. ELECTRICAL CHARACTERIZATION OF MIM STRUCTURES

Figure 4 shows $\Delta C/C_{\min}$ (V) behavior for different HfO_2 thicknesses (measured by ellipsometry) on the two different metal electrodes. Figure 5 presents the continuous electrical behavior in terms of current versus voltage. It is well known that oxide layer thickness significantly changes the overall MIM electrical properties. For instance, in the Pt case, voltage linearity is improved with the HfO_2 thickness increase while capacitance density decreases from 18 to 12 $\text{fF}/\mu\text{m}^2$, respectively, for the 5 and 11 nm films. On TiN, trends are the same, as capacitance densities evolve from 6 to 23 $\text{fF}/\mu\text{m}^2$ for 18 to 3 nm films, and voltage linearity is

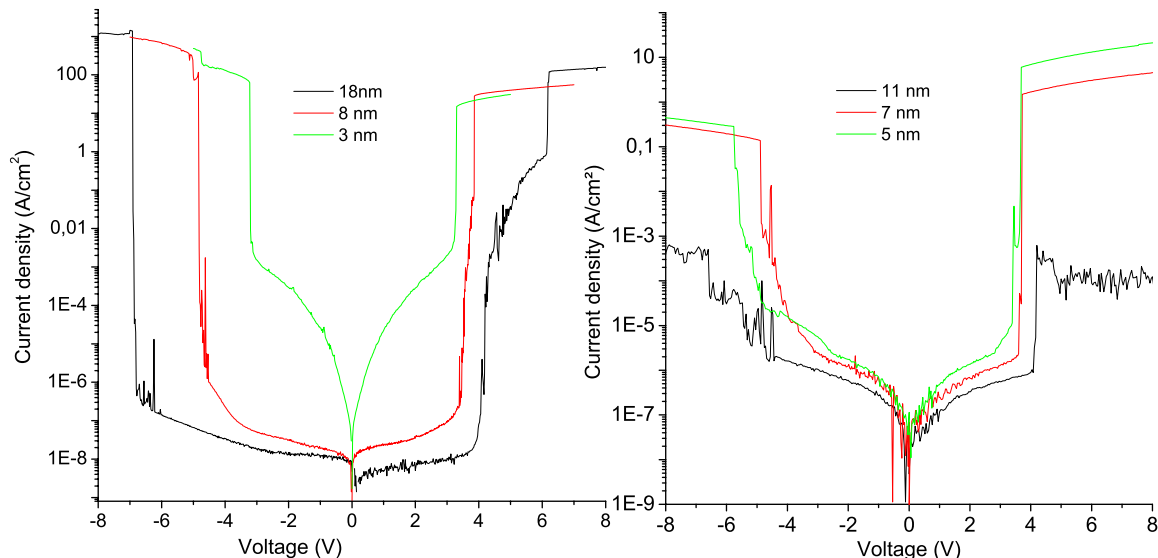


FIG. 5. (Color online) Current density vs voltage at three different HfO_2 thicknesses on TiN (left) and Pt (right).

TABLE I. Capacitance density, quadratic coefficient, dc leakage current, and dielectric losses for HfO₂ layered MIM capacitors with TiN and Pt electrodes. Values are given at 100 and 10 kHz. α are established on the positive side of the C - V curves which are mainly influenced by the bottom electrodes.

	Thickness (nm)	C_s (fF/ μm^2)		α (ppm/V ²)		Leakage (2 V) ($\mu\text{A}/\text{cm}^2$)	tan δ	
		100 kHz	10 kHz	100 kHz	10 kHz		100 kHz	10 kHz
TiN	18	6.4	6.5	500	550	0.005	0.008	0.012
	8	12.8	13.1	2620	3260	0.036	0.020	0.030
	3	21.6	23.2	$\sim 12 \times 10^5$	$\sim 12 \times 10^5$	280	0.033	0.050
Pt	11	12	12.2	2250	2450	0.5	0.015	0.015
	7	15	15.3	2750	3550	0.7	0.02	0.02
	5	18	18.6	3250	4150	1.9	0.02	0.02

significantly degrading with decreasing thickness. It has been shown by Wenger *et al.*¹⁸ that the oxidized interfacial layer is responsible for the linearity behavior degradation.

Different values of α extracted from polynomial fits of the $\Delta C/C_{\min}$ curves shown in Fig. 4 are also reported in Table I. It is seen that the 7 nm HfO₂ MIM exhibits the best compromise between high capacitance density and voltage linearity. Moreover, all the samples present very low loss tangent around 0.02 without any clear dependency on the electrode. Only the thinner (3 nm) film on TiN, which also exhibits a clear excessive leakage current, has a 0.05 loss tangent.

Using a double layer series capacitance model, we estimated the thickness of the interfacial layer (IL). For both cases we used the usual value of 18 for the monoclinic HfO₂ dielectric constant.³¹ In the TiN case we used a dielectric constant of 6 obtained by Schroeder *et al.*³² for oxynitrided TiO_xN_y interface layer. It resulted in ILs of 2.2, 1.43, and 1.37 nm for the 18, 8, and 3 nm films. In the Pt case, despite the fact that no oxidized Pt state had been seen with the XPS measurements, the spectroscopic ellipsometry showed that we had to consider the existence of an actual IL. Considering a constant monolayer of 0.5 nm, we obtained dielectric constants in the range of 3–4. This IL could be considered as the first chemical bond obtained during the first HfCl₄ ALD cycle.

We have verified the frequency evolution and the link between the conductivity and the α values in the TiN case. In the Pt case, this link is less obvious, as we observe that either the leakage current and α remain nearly constant for the three studied thicknesses. The ratio of α to C_s^2 is in the range 10–15 m⁴ V⁻² F⁻². This ratio should not depend on the oxide thickness and is a vision of the MIM potentiality. With the assumption that the electrical properties of the oxide (conductivity) are not modified when thinning it, we obtain the minimum value of α that can be reached for a capacitance density of 10 fF/ μm^2 . As an example, a value of 15 means that α should be equal to 1500 ppm/V² for $C_s = 10$ fF/ μm^2 . Hence, the objective is a α/C_s^2 parameter less or equal to 1. This parameter is also interesting since we do not have to precisely know the oxide thickness. Here we found that this ratio is kept nearly constant whatever the

HfO₂ thickness in case of Pt electrode. This can be correlated with the relative constant value of conductivity measured at 1 MV/cm from the $I(E)$ curve: its value is varying between 1.9 and 22×10^{-13} S/cm for the three thicknesses. In the case of TiN electrode, the α/C_s^2 ratio is increasing from 12 to more than 300. This is correlated with the increasing leakage currents observed when thinning the HfO₂ dielectric: the conductivity is then varying from 7×10^{-15} to 7×10^{-13} S/cm. This experimentally confirms a correlation between the quadratic parameter α and the conductivity as physically described by the electrode polarization mechanism proposed by Gonon and Vallée.¹⁶

Nevertheless, the use of a platinum electrode with HfO₂ insulated material still induces $\mu\text{A}/\text{cm}^2$ leakage currents for the planar single-layered MIM structure (see Table I), even for the 11-nm-thick sample. Moreover, on contrary to what we thought, the linearity properties are not improved in a effective way with the Pt electrode (thanks to the very thin interfacial oxide and/or its high work function value), even though it has been observed in the case of Y₂O₃ and other materials.^{8,12–14} Finally, regarding both leakage currents and linearity performances, the benefit of Pt bottom electrode is not clearly demonstrated for thick HfO₂ films. In the case of very thin HfO₂ materials (<10 nm), the constant value of α , correlated with a constant behavior for the leakage currents, has to be confirmed.

Temperature dependence of the capacitance versus voltage behavior has been verified between 25 and 125 °C for the two thicker films on each metal. The quadratic coefficient is nearly constant on TiN (3% increase at 125 °C) and increases by 30% (3%) for the 7 nm (11 nm) film(s) on Pt. This is not comparable to the variations observed by Mikhelashvili *et al.*⁹ with a laminate stack.

V. CONCLUSION

Physical and optical analyses show that the monoclinic phase of HfO₂ is more pronounced for thin films deposited on Pt electrode instead of TiN electrode. The thickness of the interfacial layer is comprised between 1.5 and 2 nm for films deposited on TiN while it is of the monolayer type in the

case of deposition on Pt electrodes. Best results for very thin HfO₂ films, i.e., very high capacitance density, in terms of voltage linearity are obtained with the platinum electrodes. This is correlated with differences observed between the continuous conductivity when using Pt electrode instead of TiN electrode. The linearity improvement for very thin HfO₂ films deposited on Pt can also be linked to the fact there is nearly no interfacial layer which appear on the platinum. Concerning the excessive leakage current measured with the Pt electrode, we may notice that the monoclinic crystallization should lead to conduction through the grain boundaries.

- ¹D. Dornisch, G. Wilk, G. Li, K.M. Ring, D.J. Howard, and Marco Racanelli, *ECS Trans.* **6**, 755 (2007).
- ²The International Technology Roadmap for Semiconductors, Semiconductor Industry Association, 2003.
- ³S. Blonkowski, M. Regache, and A. Halimaoui, *J. Appl. Phys.* **90**, 1501 (2001).
- ⁴C. Durand, C. Vallée, C. Dubourdieu, M. Kahn, M. Derivaz, S. Blonkowski *et al.*, *J. Vac. Sci. Technol. A* **24**, 459 (2006).
- ⁵H. Hu, C. Zhu, Y. F. Lu, Y. H. Wu, T. Liew, M. F. Li, B. J. Cho, W. K. Choi, and N. Yakovlev, *J. Appl. Phys.* **94**, 551 (2003).
- ⁶K. C. Chiang *et al.*, *J. Electrochem. Soc.* **154**, G54 (2007).
- ⁷Ch. Wenger *et al.*, *Microelectron. Eng.* **80**, 313 (2005).
- ⁸V. Mikhelashvili, G. Eisenstein, and A. Lahav, *Appl. Phys. Lett.* **90**, 013506 (2007).
- ⁹V. Mikhelashvili, P. Thangadurai, W. D. Kaplan, and G. Eisenstein, *Appl. Phys. Lett.* **92**, 132902 (2008).
- ¹⁰L. Goux, H. Vander Meeren, and D. J. Wouters, *J. Electrochem. Soc.* **153**, F132 (2006).
- ¹¹D. Brassard, L. Ouellet, and M. A. El Khakani, *IEEE Electron Device Lett.* **28**, 261 (2007).
- ¹²C. H. Cheng, K. C. Chiang, H. C. Pan, C. N. Hsiao, C. P. Chou, S. P. McAlister, and A. Chin, *Jpn. J. Appl. Phys., Part 1* **46**, 7300 (2007).
- ¹³F. El Kamel, P. Gonon, and C. Vallée, *Appl. Phys. Lett.* **91**, 172909 (2007).
- ¹⁴M. Kahn *et al.*, Proceeding of the 53rd American Vacuum Society (AVS) Symposium, San Francisco, 2006 (unpublished).
- ¹⁵G. Yip, J. Qiu, W. T. Ng, and Z. H. Lu, *Appl. Phys. Lett.* **92**, 122911 (2008).
- ¹⁶P. Gonon and C. Vallée, *Appl. Phys. Lett.* **90**, 142906 (2007).
- ¹⁷J. Robertson, O. Sharia, and A. A. Demkov, *Appl. Phys. Lett.* **91**, 132912 (2007).
- ¹⁸Ch. Wenger, G. Lupina, M. Lukosius, O. Seithfarth, H.-J. Müssig, S. Pasko, and Ch. Lohe, *J. Appl. Phys.* **103**, 104103 (2008).
- ¹⁹S. J. Kim *et al.*, *IEEE Electron Device Lett.* **25**, 538 (2004).
- ²⁰M. Kahn *et al.*, *Microelectron. Reliab.* **47**, 773 (2007).
- ²¹Y. Morisaki, Y. Sugita, K. Irino, and T. Aoyama, IWGI, Tokyo, 2001.
- ²²F. Ferrieu, K. Dabertrand, S. Lhostis, V. Ivanova, E. Martinez, C. Licitra, and G. Rolland, *J. Non-Cryst. Solids* **353**, 658 (2007).
- ²³J. F. Moulder, W. F. Stickle, P. E. Sobol, and K. Bomben, *Handbook of X-ray Photoelectron Spectroscopy*, 2nd ed., edited by J. Chastain (Perkin-Elmer, Eden Prairie, MN, 1992).
- ²⁴G. E. Jellison, Jr. and F. A. Modine, *Appl. Phys. Lett.* **69**, 371 (1996); **69**, 2137 (1996).
- ²⁵P. Boher, P. Evrard, O. Condat, C. Dos Reis, C. Defranoux, J. Ph. Piel, J. L. Stehle, and E. Bellandi, *Thin Solid Films* **455–456**, 798 (2004).
- ²⁶N. V. Nguyen *et al.*, *J. Vac. Sci. Technol. A* **23**, 1706 (2005).
- ²⁷C. Licitra, E. Martinez, N. Rochat, T. Veyron, H. Grampeix, M. Gely, J. P. Colonna, and G. Molas, *AIP Conf. Proc.* **931**, 292 (2007).
- ²⁸F. L. Martinez, M. Toledano-Luque, J. J. Gandia, J. Carabe, W. Bohne, J. Röhrich, E. Strub, and I. Martil, *J. Phys. D* **40**, 5256 (2007).
- ²⁹Y. J. Cho, N. V. Nguyen, C. A. Richter, J. R. Ehrstein, B. H. Lee, and J. C. Lee, *Appl. Phys. Lett.* **80**, 1249 (2002).
- ³⁰G. Lucovsky and J. Lüning, Proceedings of ESSDERC Grenoble, France, 2005 (unpublished), Vol. 439.
- ³¹X. Zhao and D. Vanderbilt, *Phys. Rev. B* **65**, 233106 (2002).
- ³²T. Schroeder, G. Lupina, R. Sohal, G. Lippert, Ch. Wenger, O. Seifarth, M. Tallarida, and D. Schmeisser, *J. Appl. Phys.* **102**, 014103 (2007).